Extended interacting boson model with configuration mixing description for ^{98}Mo

Feng Pan [1,2,*] Lianrong Dai [3,†] Jerry P. Draayer,[2,‡] and David Kekejian[4,§]

[1]*Department of Physics, Liaoning Normal University, Dalian 116029, China*

[2]*Department of Physics and Astronomy, Louisiana State University, Baton Rouge, Louisiana 70803-4001, USA*

[3]*Department of Physics, School of Science, Huzhou University, Huzhou, Zhejiang 313000, China*

[4]*Department of Physics and Astronomy, University of North Carolina, Chapel Hill, North Carolina 27599, USA*

(Received 22 December 2023; revised 4 March 2024; accepted 18 April 2024; published 6 May 2024)

An extended version of the interacting boson model (IBM), encompassing two-particle–two-hole (2p-2h) excitations originating from below a valence shell and one-particle–one-hole (1p-1h) excitations extending to the upper next-nearest major shell, is developed to investigate cross-shell excitation effects in the transitional nucleus ^{98}Mo. This extended IBM framework is utilized to reproduce experimentally observed properties such as low-lying positive-parity level energies, $B(E2)$ values, and the electric quadrupole moment of the 2_1^+ state, $\rho^2(E0, 0_2^+ \to 0_g^+)$, as well as the strength functions of the isoscalar giant monopole resonance (ISGMR) and the isoscalar giant quadrupole resonance (ISGQR) in ^{98}Mo. It is shown that the extended consistent-Q IBM, incorporating configuration mixing of both 2p-2h excitations from below the valence shell and 1p-1h excitations to the upper next-nearest major shell, describes the low-lying structural properties and the ISGMR and ISGQR strength distributions of ^{98}Mo quite well, with the ISGMR and the ISGQR strength distributions comparable to the results of the self-consistent quasiparticle random-phase approximation with Skyrme interactions.

DOI: 10.1103/PhysRevC.109.054306

I. INTRODUCTION

It is evident that, besides the collective model [1], the interacting boson model (IBM) has been successful in describing low-lying spectra of medium- and heavy-mass nuclei [2,3]. Configuration-mixing (CM) schemes based on the IBM that include multiple two-particle and two-hole (2p-2h) excitations from below a valence shell have also been successfully established [4,5] in elucidating intruder states and shape coexistence phenomena for nuclei near to a closed shell [6]. On the other hand, the dynamical symmetry of the three-dimensional harmonic oscillator (3D-HO) can be extended from the U(3) group to a noncompact Sp(3,R) group to accommodate multiple one-particle–one-hole (1p-1h) excitations. Actually, such 1p-1h excitations are included in the nuclear shell model when cross-shell terms of the quadrupole operators are taken into account, while those cross-shell terms are neglected in valence shell model calculations and the original IBM. The symplectic extension in the collective model framework was made by Rosensteel and Rowe in the later seventies [7]. The link between the Sp(3,R) collective model with a natural extension of the Elliott SU(3) shell model was also clearly established [8].

Inspired by the Sp(3,R) collective model [7] and the recent work on the *ab initio* Sp(3,R) symmetry-adapted no-core shell model calculations for light nuclei [9–11], very recently, a similar multishell extension of the consistent-Q (CQ) formalism of the IBM has been made [12], in which a series of 1p-1h excitations to the upper next-nearest major shell with the 1p-1h pairs being approximated as bosons is taken into account. The extended IBM was applied to describe low-lying excitations, the isoscalar monopole resonance (ISGMR), and the isoscalar quadrupole resonace (ISGQR) of ^{152}Sm. The results show that the widely populated ISGMR and ISGQR strengths of ^{152}Sm cannot be well reproduced by the model. In this work, the previous multishell extension [12] of the CQ-IBM with further configuration mixing of 2p-2h excitations from below the valence shell is applied to the transitional nucleus ^{98}Mo.

II. THEORETICAL FRAMEWORK

The extended CQ-IBM Hamiltonian is written as

$$\hat{H} = \sum_{k=0}^{1} \hat{P}_{N+2k}\, \hat{H}_{0,k}\, \hat{P}_{N+2k} + \hat{P}_{N+2}\hat{H}_{\rm mix}\hat{P}_N + \hat{P}_N\hat{H}_{\rm mix}\hat{P}_{N+2} + \epsilon_S\, \hat{n}_S + \epsilon_D\, \hat{n}_D + a\ \hat{L}\cdot\hat{L}, \tag{1}$$

with

$$\hat{H}_{0,k} = \delta_{k1}\Delta + \epsilon_{d,k}\, \hat{n}_d - \kappa_k\, \hat{Q}(k)\cdot\hat{Q}(k), \tag{2}$$

where k labels the $2k$-particle and $2k$-hole excitations in an even-even nucleus considered; $\hat{P}_{N+2k}$ is the projection operator independent of the S and D bosons, which projects into the $N+2k$ configuration of s and d bosons; $\hat{n}_d = d^\dagger\cdot\tilde{d}$ ($\hat{n}_S = S^\dagger S$ and $\hat{n}_D = D^\dagger\cdot\tilde{D}$) are the number operators of the

*daipan@dlut.edu.cn
†dailianrong@zjhu.edu.cn
‡draayer@lsu.edu
§kekejian@unc.edu

d bosons (the S and D bosons), respectively; $\epsilon_{d,k}$ are the single-particle energies of the s and d bosons in the $N+2k$ configurations; ϵ_S and ϵ_D are the single-particle energies of the S and D bosons; κ_k ($k=0$ or 1) are the quadrupole-quadrupole interaction strengths;

$$\hat{Q}_\mu(k) = \alpha(D^\dagger_\mu + \tilde{D}_\mu) + \hat{Q}^{(0)}_\mu(k) + \hat{Q}^{(1)}_\mu(k), \tag{3}$$

in which α is a dimensionless parameter,

$$\hat{Q}^{(0)}_\mu(k) = d^\dagger_\mu s + s^\dagger \tilde{d}_\mu + \chi_k(d^\dagger \times \tilde{d})^{(2)}_\mu, \tag{4}$$

$$\hat{Q}^{(1)}_\mu(k) = D^\dagger_\mu S + S^\dagger \tilde{D}_\mu + \chi'_k(D^\dagger \times \tilde{D})^{(2)}_\mu, \tag{5}$$

$$\hat{H}_{\rm mix} = g_s(s^{\dagger\,2} + s^2) + g_d(d^\dagger \cdot d^\dagger + \tilde{d} \cdot \tilde{d}), \tag{6}$$

in which g_s and g_d are the N and $N+2$ configuration mixing parameters; $\Delta = \Delta_0 + \epsilon_{s,1}(N+2)$, with Δ_0 being the energy required to excite two particles from the nearest lower shell resulting in 2p-2h excitations and $\epsilon_{s,1}$ being the single-particle energy of the s-bosons in the $N+2$ configuration; and the last $\hat{L}\cdot\hat{L}$ term in Eq. (1) is added to get a better fit to the low-lying level energies. The S and D bosons are approximations from 1p-1h pairs with one particle in the upper next-nearest shell and one hole in the valence shell [12], of which the single-particle energies are expressed as

$$\epsilon_S = \epsilon^{(0)}_S + 2\,\hbar\omega, \quad \epsilon_D = \epsilon^{(0)}_D + 2\,\hbar\omega, \tag{7}$$

with $2\hbar\omega = 82\,A^{1/3}$ MeV, which gives $2\hbar\omega = 17.786$ MeV for ^{98}Mo. It is clearly shown in the IBM-CM calculations [4,5] that the projection operator $\hat{P}_{N+2k}$ in the first term of Eq. (1) is used to define different shapes characterized by the k-dependent model parameters of $\hat{H}_{0,k}$ related to the normal ($k=0$) and intruder ($k=1$) configurations. Since the dimensionless parameter α in the 1p-1h pair mixing term $\alpha(D^\dagger_\mu + \tilde{D}_\mu)$ shown in Eq. (3) has nothing to do with the normal ($k=0$) and intruder ($k=1$) configurations, like the $\epsilon_S\,\hat{n}_S + \epsilon_D\,\hat{n}_D$ term in the Hamiltonian (1), the dimensionless parameter α in the 1p-1h pair mixing term $\alpha(D^\dagger_\mu + \tilde{D}_\mu)$ shown in Eq. (3) should be independent of k. Moreover, the $s^{\dagger\,2} + s^2$ and $d^\dagger \cdot d^\dagger + \tilde{d}\cdot\tilde{d}$ terms in $\hat{H}_{\rm mix}$ are equivalent to the effective monopole-pairing and quadrupole-pairing interactions of the particle pairs in the valence shell with the hole pairs in the lower nearest shell. Therefore, $g_s < 0$ may be more appropriate. Nevertheless, as analytically verified for the U(5) and O(6) limit cases [13], the eigenenergies of the Hamiltonian (1) are independent of the sign of g_s and g_d, which may be the reason for assuming $g_s > 0$ and $g_d > 0$ instead in previous studies [4–6,14,15]. Similarly, $g_s = g_d = g > 0$ is taken in the present fitting scheme. The Hamiltonian (1) with no 2p-2h configuration mixing and no distinction of the S and D bosons from the s and d bosons is reduced to the hydrodynamic limit [16–18] of the symplectic collective model [7].

As shown in our previous work [12], there is less contribution from configurations of $2n\hbar\omega$ excitations above the valence shell for $n \geqslant 2$ to the eigenstates of the model. In this work, we only consider 1p-1h excitations with approximately $2\hbar\omega$ in energy to the upper next-nearest major shell in the configuration mixing scheme of the valence shell with 2p-2h excitations from below the valence shell in the extended CQ-IBM framework. The Hamitonian (1) is diagonalized in the SO(3) coupled U(6) $\supset$ U(5) $\supset$ O(5) $\supset$ SO(3) basis of the s and d bosons and that of the S and D bosons with

$$\begin{aligned}|N+2k,\ n_d\ v\ \eta\ L_d;\ \mathscr{N},\ n_D\ v_D\ L_D; L\,M\rangle \\ = \sum_{M_d,\,M_D} \langle L_d\,M_d,\ L_D\,M_D|L\,M\rangle \\ \times |N+2k,\ n_d\ v\ \eta\ L_d\,M_d; \mathscr{N},\ n_D\ v_D\ L_D\,M_D\rangle\end{aligned} \tag{8}$$

for $k=0$ or 1 and $\mathscr{N}=0$ or 1, where N ($\mathscr{N}$) is the total number of s and d bosons (S and D bosons); n_d (n_D), v_d (v_D), and L_d (L_D) are the number of the d bosons (D bosons), the seniority number of the d bosons (D bosons), and the angular momentum quantum number of the d bosons (D bosons), respectively; η is the O(5) $\supset$ O(3) branching multiplicity label; and $\langle L_d\,M_d,\ L_D\,M_D|L\,M\rangle$ is the SO(3) Clebsch-Gordan coefficient. Configuration mixing of more S and D bosons with $\mathscr{N} \geqslant 2$ is not considered in this work due to the fact that the $\mathscr{N} \geqslant 2$ contribution to the low-lying states of the model is negligible [12].

The $E2$ transition operators in the present model are taken as

$$T_\mu(E2) = \sum_{k=0}^{1} q_{2,k}\,\hat{P}_{N+2k}\,\hat{Q}_\mu(k)\,\hat{P}_{N+2k}, \tag{9}$$

with the quadrupole operator $\hat{Q}_\mu(k)$ shown in Eq. (3), in which the parameter α is mainly determined by the ISGQR, where $q_{2,k}$ is the effective charge related parameter for each configuration. Similarly, the $E0$ transition operator is taken as

$$T(E0) = \sum_{k=0}^{1} \beta_{0,k}\hat{P}_{N+2k}\,\hat{n}_s\,\hat{P}_{N+2k} + \beta(S^\dagger + S). \tag{10}$$

In the present calculation, $q_{2,0} = q_{2,1} = q_2$ and $\beta_{0,0} = \beta_{0,1} = \beta_0$ are taken to reduce the number of free parameters. In Eq. (11), β_0 is fixed by the experimentally known $B(\mathrm{E0}; 0^+_2 \to 0^+_{\rm g})$ strength, while β is mainly determined by the ISGMR strength distribution.

III. THE MODEL FIT TO ^{98}Mo

Experimentally known positive-parity level energies below the 6^+_1 level at 2.343 MeV, $B(E2)$ values, the electric quadrupole moment of the first 2^+ state, $\rho^2(E0, 0^+_2 \to 0^+_{\rm g})$,

TABLE I. Model parameters (in MeV) for ^{98}Mo, where $\kappa_1 = \kappa_0$, the dimensionless parameters $\chi_1 = \chi_0 = \chi'_1 = \chi'_0$ and α, and the effective charge parameters q_2 and β_0 and β used in Eqs. (9) and (10), respectively.

$\epsilon_{d,0} = 1.164$	$\kappa_0 = 0.0069$	$\chi_0 = -0.164$	$\epsilon_{d,1} = 0.499$	$\Delta = 0.374$	$g = 0.07$	$a = 0.005$
$\epsilon^{(0)}_S = -1.586$	$\epsilon^{(0)}_D = -4.586$	$\alpha = 3.88$	$q_2 = 0.1015\ e$ b	$\beta_0 = 0.011\ e$ b	$\beta = 0.686\ e$ b	

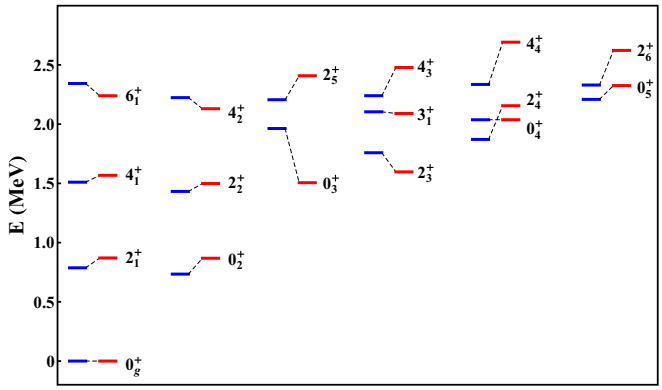

FIG. 1. Experimentally identified 17 positive-parity level energies (in MeV) below 2.343 MeV of ^{98}Mo fitted by the present model, where the left (blue) levels are those observed in experiments [25], and the right (red) levels are those obtained from the present model.

and the ISGMR and ISGQR strength distributions of ^{98}Mo are systematically fitted by the present model. In the previous IBM configuration-mixing calculations for ^{98}Mo, the Hamiltonian is diagonalized within the IBM-II $([N_\pi] \oplus [N_\pi + 2]) \otimes [N_\nu]$ subspace with $N_\pi = 1$ and $N_\nu = 3$ [14] or equivalently in the IBM $[N] \oplus [N + 2]$ subspace with $N = 4$ [15]. In the present work, the extended CQ-IBM calculation, including both the 2p-2h excitations from below the valence shell and the 1p-1h excitations to the upper next-nearest shell, is performed. Namely, the Hamiltonian (1) is diagonalized within the $V \otimes [\mathcal{N} = 0] \oplus V \otimes [\mathcal{N} = 1]$ subspace with the basis vectors shown in Eq. (8), where $V = [N] \oplus [N + 2]$, with $N = 4$.

In order to further reduce the number of parameters, $\kappa_1 = \kappa_0$ and $\chi_1' = \chi_0' = \chi_1 = \chi_0$ are set. Since the parameters α, ϵ_S, ϵ_D, and β are sensitive to the ISGMR and ISGQR strength functions, while the parameter χ_0 is sensitive to the electric quadrupole moment $Q(2_1^+)$, the model parameters are determined by a best fit to the low-lying level energies, the ISGMR and ISGQR strength functions, and the electric quadrupole moment $Q(2_1^+)$. During the fit, the effective-charge-related parameters q_2 and β_0 are fixed by the experimental value of $B(E2, 2_1^+ \to 0_g^+)$ and $10^3\,\rho^2(E0, 0_2^+ \to 0_g^+)$ [19], respectively, while χ_0 is mainly determined by the experimental value of $Q(2_1^+)$. The parameters produced from the best fit are provided in Table I. In the IBM, the nuclear shape in each configuration is mainly determined by the ratio $\epsilon_{d,k}/\kappa_k$ for given χ_k in the CQ formalism [20,21]. Therefore, only $\epsilon_{d,0}/\epsilon_{d,1}$ measures the shape difference of the normal $[N]$ configuration from that of the intruder $[N + 2]$ configuration in the present fitting scheme. It should be noted that $\Delta = 0.374$ MeV is determined from the best fit to the low-lying level energies, which is far less than the excitation energy of two protons from below the $Z = 40$ subshell used in the previous analysis [14,15]. The Δ value of the present fit, which is smaller than that used the previous analysis [14,15], is equivalently due to stronger attractive monopole pairing in the $[N + 2]$ configuration being adopted with larger $|\epsilon_{s,1}|$ in the present calculation, where $\epsilon_{s,1} < 0$ is assumed. Except that the shape of the normal configuration determined by the present and previous calculations are quite similar, which is almost spherical, the major difference of the present fitting results from those of previous calculations lies in the fact that the shape of the intruder $[N + 2]$ configuration is still near to the U(5) (spherical) point with $\epsilon_{d,1}/\kappa_1 = 72.32$ and $\chi_1 = -0.164$ in the present model in contrast to that mixed with an oblate deformed shape with $\epsilon_{d,1}/\kappa_1 = 34.817$ and $\chi_1 = 1.5$ shown in Ref. [15]. The ratio $\epsilon_{d,0}/\epsilon_{d,1} = 2.33$ obtained from the present fitting scheme indicates that the shape of the intruder $[N + 2]$ configuration in the present model is a little away from the U(5) (spherical) towards slightly prolate deformed with $\chi_1 = -0.164$.

As mentioned previously, the parameters α, ϵ_S, ϵ_D, and the $E0$ effective charge parameter β shown in Eq. (10) are sensitive to and mainly determined by the ISGMR and ISGQR strength functions of the excitation energy E_x defined by [22,23]

$$S_\lambda(E_x) = \frac{\Gamma}{2\pi} \sum_\xi \frac{(2\lambda + 1)|\langle \xi; \lambda || T(\mathrm{E}\lambda) || 0 \rangle|^2}{(E_x - E_\xi)^2 + \frac{\Gamma^2}{4}}, \qquad (11)$$

where $|0\rangle$ stands for the ground state, $|\xi; \lambda\rangle$ stands for $L^\pi = \lambda^+$ excited states of the model with the corresponding energy E_ξ, and the folding width $\Gamma = 2.5$ MeV [24] is used. The fitting to the experimental data of $\lambda = 0$ and $\lambda = 2$ strength functions of ^{98}Mo yields $\alpha = 3.88$, $\epsilon_S^{(0)} = -1.586$ MeV, $\epsilon_D^{(0)} = -4.586$ MeV, and $\beta = 0.686\,e\,\mathrm{b}$.

TABLE II. $B(E2, L_\mathrm{i} \to L_\mathrm{f})$ values (in W.u.), where * indicates that the corresponding value is fixed according to the experimental data. Specifically, q_2 and β_0 are fixed by $B(E2, 2_1^+ \to 0_\mathrm{g}^+)$ and $10^3\,\rho^2(E0, 0_2^+ \to 0_\mathrm{g}^+)$ [19] shown in the last row of the Table, respectively, and χ_0 is fixed by the electric quadrupole moment $Q(2_1^+)$ (in e b).

	Expt. [25]	Present model		Expt. [25]	Present model
$2_1^+ \to 0_\mathrm{g}^+$	20.1 (4)	20.1*	$2_3^+ \to 4_1^+$	14.4 (4)	2.84
$4_1^+ \to 2_1^+$	$42.3^{\,0.9}_{-0.8}$	42.16	$2_2^+ \to 0_\mathrm{g}^+$	$1.02^{\,0.15}_{-0.12}$	0.004
$6_1^+ \to 4_1^+$	10.1(4)	53.23	$2_3^+ \to 0_\mathrm{g}^+$	$0.032^{\,0.007}_{-0.006}$	1.36
$2_1^+ \to 0_2^+$	$9.7^{\,1.0}_{-2.5}$	4.21	$2_3^+ \to 2_1^+$	3.0 (7), 1.07(2) [26]	0.00
$2_2^+ \to 0_2^+$	$2.3^{\,0.5}_{-0.4}$, 4.69 (1) [26]	0.01	$2_2^+ \to 2_1^+$	$48^{\,9}_{-8}$, 4.66 (4) [26]	41.97
$2_3^+ \to 0_2^+$	$7.5^{\,0.6}_{-0.5}$	15.93	$4_1^+ \to 2_2^+$	$15.2^{\,3.3}_{-3.0}$, 3.73 (2) [26]	0.07
$Q(2_1^+)$	−0.26 (9), −0.045 (23) [26]	−0.045*	$0_2^+ \to 0_\mathrm{g}^+$	27.3 (11)	27.3*

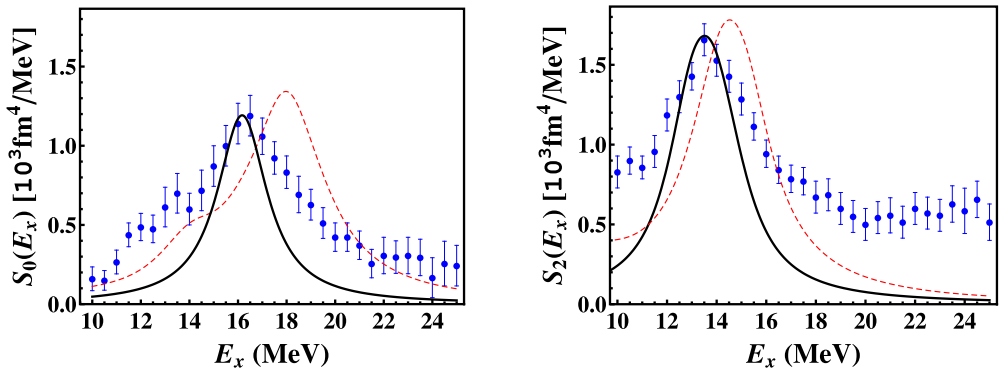

FIG. 2. The $\lambda = 0$ and $\lambda = 2$ strength distributions of ^{98}Mo, where the blue dots with error bars are the experimental data extracted from Refs. [27,28], the (red) dashed curves are the results of the self-consistent quasiparticle random-phase approximation (QRPA) approach with Skyrme interactions provided by the authors of Ref. [24], and the (black) solid curves are produced from the present model.

As shown in Fig. 1, except for the 4_4^+ and 2_4^+ level energies being about 357 and 285 keV too high in the present model, respectively, which also leads to the ordering of the 2_4^+ and 0_4^+ levels reversed in the present model, and the energy gap between the 2_5^+ and 0_3^+ levels being about 660 keV too large in comparison to the experimental data, all the other experimentally observed positive-parity level energies below 2.343 MeV are well fit. The root-mean-square deviation of the model fitting to the 17 positive-parity level energies shown in Fig. 1 is 203.1 keV.

Table II provides the $B(E2)$ values of ^{98}Mo obtained from the present model with the model parameters thus fixed, in which only experimentally known $B(E2)$ values are shown. Except for $B(E2, 6_1^+ \to 4_1^+)$, of which the present model result is about 5 times larger than the corresponding experimental value, the overall data pattern of the fitting results follows that of the experimental data. It should be noted that the $B(E2, 6_1^+ \to 4_1^+)$ value obtained from the present model is very close to that calculated from a similar IBM configuration-mixing scheme shown in Ref. [26]. Moreover, $B(E2, 2_2^+ \to 2_1^+)$ obtained in the present model is very close to the previous experimental value, while $B(E2, 4_1^+ \to 2_2^+)$ is close to the experimental result provided in Ref. [26]. It is obvious that the recent experimental $Q(2_1^+)$ value [26] differs noticeably from the previous one [25]. The systematic present model fit prefers to the $Q(2_1^+)$ result shown in Ref. [26] with a slightly prolate deformed shape, to which the χ_0 value of the present model is fixed.

Figure 2 provides the ISGMR and ISGQR strength functions fitted by the present model in comparison to the results of the self-consistent quasiparticle random-phase approximation (QRPA) approach with Skyrme interactions [24]. It is shown that, though the results of the present model are still insufficient in widths, the present extended IBM calculation in taking account of the 2p-2h configuration mixing can produce the ISGMR and ISGQR strength distributions with the results similar to those of the QRPA [24]. To demonstrate the 2p-2h configuration mixing effect on the strength functions, both the $\lambda = 0$ and $\lambda = 2$ strength functions produced from the present model are compared with the corresponding ones produced from the same model with the same parameters in the $[N]$ configuration but without the 2p-2h configuration and the mixing. It is shown that the $\lambda = 0$ strength function in the present model and that in the same model with the same parameters in the $[N]$ configuration but without the 2p-2h configuration and the mixing are almost the same, while the width of the the $\lambda = 2$ strength function in the present model is a little larger as shown in Fig. 3, which indicates that the 2p-2h configuration mixing makes the $\lambda = 2$ strength distribution a little broadening, but keeps the $\lambda = 0$ strength function almost unchanged. It should be noted that the results of the present model without the 2p-2h configuration and the mixing is used for comparison only, of which the low-lying spectrum becomes incomparable to the experimental result.

It can be observed from Eqs. (8) and (10) that the contribution to the $\lambda = 0$ strength function is mainly from the reduced matrix element

$$\langle N + 2k,\ n_d\ v\ \eta\ 0;\ \mathscr{N} = 1,\ 0\,0\,0;\ 0||S^\dagger||N + 2k,\ n_d\ v\ \eta\ 0;\ \mathscr{N} = 0,\ 0\ 0\,0;\ 0\rangle, \tag{12}$$

with $k = 0$ only, because the ground state is normal configuration dominated, which answers why the $\lambda = 0$ strength function in the present model and that in the same model

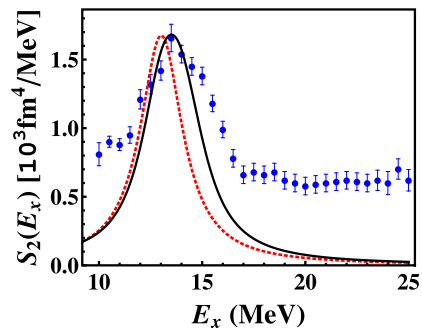

FIG. 3. The $\lambda = 2$ strength distribution of ^{98}Mo, where the (red) dotted curve is the result of the present model with the same parameters in the $[N]$ configuration but without the 2p-2h configuration and the mixing, the (black) solid curve is produced from the present model as shown in Fig. 2, and the experimental data (blue dots with error-bars) are also shown for comparison.

TABLE III. $(N+2k;\mathscr{N}=0)$ and $\mathscr{N}=1$ configuration contributions to the excited states of ^{98}Mo in the present model.

Configuration	0_g^+	0_2^+	0_3^+	2_1^+	2_2^+	2_3^+	4_1^+	4_2^+	6_1^+
$\upsilon(N)$	0.672 410	0.300 641	0.093 491	0.264 928	0.057 558	0.601 917	0.300 641	0.672 410	0.012 686
$\upsilon(N+2)$	0.327 488	0.699 257	0.906 343	0.734 462	0.941 768	0.397 719	0.699 257	0.327 488	0.986 677
$\upsilon(\mathscr{N}=1)$	0.000 102	0.000 102	0.000 166	0.000 610	0.000 674	0.000 364	0.000 102	0.000 102	0.000 637

without the 2p-2h configuration and the mixing are almost the same. Similarly, the contribution to the $\lambda=2$ strength function is mainly from the reduced matrix elements

$$\alpha\,\langle N+2k,\ n_d\,\upsilon\,\eta\,0;\ \mathscr{N}=1\,1\,1\,2;\\ 2||D^\dagger||N+2k,\ n_d\,\upsilon\,\eta\,0;\mathscr{N}=0,\ 0\ 0\,0;0\rangle. \tag{13}$$

Though the contribution from the reduced matrix elements $\langle N+2,\ n_d\,\upsilon\,\eta\,0;\ \mathscr{N}=1\,1\,1\,2;2||D^\dagger||N+2,\ n_d\,\upsilon\,\eta\,0;\ \mathscr{N}=0,\ 0\ 0\,0;0\rangle$ are suppressed due to the ground state being normal configuration dominated, the contribution from Eq. (13) with $k=1$ and $\alpha=3.88$ to the $\lambda=2$ strength function is non-negligible due to α being large for ^{98}Mo, which answers why the width of the $\lambda=2$ strength function shown in Fig. 3 is a little larger in the present model with the 2p-2h configuration mixing.

The centroid energy E_c of the ISGMR or ISGQR, defined by

$$E_c=m_1/m_0,\ \ m_k=\int_{E_a}^{E_b}E^kS_\lambda(E)dE, \tag{14}$$

is also calculated, where $[E_a,E_b]$ is taken to be that used in the experimental analysis [27,28]. The present model yields $E_c^{\rm GMR}=16.32$ MeV and $E_c^{\rm GQR}=14.41$ MeV, which are close to the experimental results shown in Refs. [27,28] with $E_{c,\rm exp}^{\rm GMR}=16.2\pm0.2$ MeV and $E_{c,\rm exp}^{\rm GQR}=14.2\pm0.1$ MeV.

The reduced matrix element of the mixing term in the Hamiltonian (1) between the $\mathscr{N}=0$ configuration and the $\mathscr{N}=1$ configuration is given by

$$\begin{aligned}&-\kappa_0\alpha\langle N+2k,\ n_d'\,\tau'\,\eta'\,L;\ \mathscr{N}=0,\ 0\ 0\,0;L\|(\hat{Q}^{(0)}(k)\cdot\tilde{D}+\tilde{D}\cdot\hat{Q}^{(0)}(k))\|N+2k,\ n_d\,\tau\,\eta\,L_0;\mathscr{N}=1,\ 1\,1\,2;L\rangle\\ &=-\kappa_0\alpha\langle N+2k,\ n_d\,\tau\,\eta\,L_0;\mathscr{N}=1,\ 1\,1\,2;L\|(\hat{Q}^{(0)}(k)\cdot D^\dagger+D^\dagger\cdot\hat{Q}^{(0)}(k))\|N+2k,\ n_d'\,\tau'\,\eta'\,L;\ \mathscr{N}=0,\ 0\ 0\,0;L\rangle\\ &=-2\kappa_0\alpha\langle N+2k,\ n_d'\,\tau'\,\eta'\,L\|\hat{Q}^{(0)}(k)\|N+2k,\ n_d\,\tau\,\eta,\ L_0\rangle\sim-0.054(N+2k),\end{aligned} \tag{15}$$

with $N=4$ for $k=0$ or 1 and for a given angular momentum quantum number L, which shows that the mixing between the $\mathscr{N}=0$ and $\mathscr{N}=1$ configurations is very small for ^{98}Mo. Similarly, the order of magnitude of reduced matrix elements of the mixing term between the $\mathscr{N}=1$ and $\mathscr{N}=2$ configurations is quite the same. Moreover, one can deduce that reduced matrix elements of the mixing term $-\kappa_0\alpha^2(D^\dagger\cdot D^\dagger+\tilde{D}\cdot\tilde{D})$ between the $\mathscr{N}=0$ and $\mathscr{N}=2$ configurations is about $-2\kappa_0\alpha^2\approx-0.21$ MeV for ^{98}Mo, which is also negligible in comparison to the $4\hbar\omega$ energy gap between the $\mathscr{N}=0$ and $\mathscr{N}=2$ configurations. Hence, the truncation with $\mathscr{N}\leqslant1$ made in this work is justified.

Table III provides $(N+2k;\mathscr{N}=0)$ and $\mathscr{N}=1$ configuration contributions to the excited states defined by

$$\upsilon(N+2k,L_\xi)=\sum_\rho|\langle N+2k;\ \mathscr{N}=0,\ \rho,\ L|L_\xi\rangle|^2 \tag{16}$$

and

$$\upsilon(\mathscr{N}=1,L_\xi)=\sum_{k=0}^{1}\sum_\rho|\langle N+2k;\ \mathscr{N}=1,\ \rho,\ L|L_\xi\rangle|^2, \tag{17}$$

where ρ stands for all the additional quantum numbers needed, $|L_\xi\rangle$ is the ξth excited state of the model with angular momentum quantum number L, and $|N+2k;\ \mathscr{N},\ \rho,\ L\rangle$ are the SO(3) coupled basis vectors shown in Eq. (8). It is clearly shown that the $(N+2k;\mathscr{N}=0)$ configuration always dominates in the excited states of the model. There is only 0.01–0.06% contribution from the $\mathscr{N}=1$ configuration to the low-lying states listed in Table III. Hence, the low-lying spectrum below $2\hbar\omega$ in energy is almost decoupled from the upper part of the spectrum containing 1p-1h excitations when $\kappa_0\alpha$ is small. Therefore, the mixing terms between the $\mathscr{N}=0$ and $\mathscr{N}=1$ configurations can also be neglected when $\kappa_0\alpha$ is small, which makes the Hamiltonian (1) in the $V\otimes[\mathscr{N}=0]\oplus V\otimes[\mathscr{N}=1]$ subspace block-diagonalized to simplify the diagonalization process. Though the configuration mixing with the 1p-1h excitations almost does not alter the properties of the low-lying states in the present model, it is essential for elucidating the ISGMR and ISGQR phenomena.

IV. CONCLUSIONS

In summary, the multishell extension of the CQ-IBM with 2p-2h excitations from the lower nearest shell and 1p-1h excitations to the upper next-nearest major shell guided by the Sp(3,R) structure is made to elucidate cross-shell excitation effects of both the low-lying spectrum and the ISGMR and ISGQR in the transitional nucleus ^{98}Mo. The extended IBM is applied to fit the experimentally known low-lying positive-parity level energies up to 2.343 MeV, $B(E2)$ values, the electric quadrupole moment $Q(2_1^+)$, $\rho^2(E0,0_2^+\to0_g^+)$, and the ISGMR and ISGQR strength functions of ^{98}Mo. It

is shown that, though the widths of the ISGMR and ISGQR peaks obtained in the present model are still insufficient, the extended consistent-Q IBM with configuration mixing of both 2p-2h excitations from the lower nearest shell and 1p-1h excitations to the upper next-nearest major shell describes the low-lying structural properties and the ISGMR and the ISGQR strength distributions of ^{98}Mo fairly well with the results of the ISGMR and the ISGQR strength distributions comparable to those of the QRPA with Skyrme interactions [24]. While the incorporation of configuration mixing involving 1p-1h excitations is crucial for understanding the ISGMR and ISGQR phenomena, its impact on the properties of low-lying states within the current model can be neglected. Specifically, the spectrum below $2\hbar\omega$ in energy remains largely unaffected and appears almost disconnected from the upper spectrum, which includes 1p-1h excitations, when $\kappa_0\alpha$ is small. Consequently, the mixing terms between the $\mathscr{N}=0$ and $\mathscr{N}=1$ configurations in the Hamiltonian in this case can be neglected, simplifying the diagonalization process of the Hamiltonian (1) within the $V\otimes[\mathscr{N}=0]\oplus V\otimes[\mathscr{N}=1]$ subspace through block diagonalization. Furthermore, in addition to the configuration mixing with multiple 2p-2h excitations from below the valence shell, exploring the extension of the IBM-II framework to incorporate both neutron and proton types of S and D bosons in the upper next-nearest shell appears to be a promising avenue for further investigation.

ACKNOWLEDGMENTS

The authors are very much grateful to the referee for helpful comments and suggestions and to Professor Gianluca Colò from Università degli Studi di Milano, Italy, and Professor Valentin O. Nesterenko from Joint Institute for Nuclear Research, Russia, for providing their QRPA results of the ISGMR and ISGQR strength distributions of ^{98}Mo. Support from the National Natural Science Foundation of China (Grants No. 12175097 and No. 12175066) and from LSU through its Sponsored Research Rebate Program as well as the LSU Foundation's Distinguished Research Professorship Program is acknowledged.

APPENDIX: MATRIX ELEMENTS IN THE U(6) ⊃ U(5) ⊃ O(5) ⊃ SO(3) BASIS

Since we adopt the U(6) ⊃ U(5) ⊃ O(5) ⊃ SO(3) basis in the calculation, matrix elements of the $\hat{n}_d$ or $\hat{n}_D$ operator can easily be read out from the coupled basis (8) for given n_d and n_D, while $\hat{n}_s = N+2k-\hat{n}_d$ when it is projected into $N+2k$ subspace and $\hat{n}_S = 1-\hat{n}_D$ in the $\mathscr{N}=1$ configuration. Using the Racah factorization lemma [29], we have that

$$\langle N'\, n_d'\, \tau'\, \eta'\, L' \| d^\dagger \| N\, n_d\, \tau\, \eta\, L\rangle = \sqrt{N+1}\left\langle \begin{matrix} N, & 1 \\ n_d & 1 \end{matrix} \middle| \begin{matrix} N+1 \\ n_d+1 \end{matrix} \right\rangle \left\langle \begin{matrix} n_d, & 1 \\ \tau & 1 \end{matrix} \middle| \begin{matrix} n_d+1 \\ \tau' \end{matrix} \right\rangle \left\langle \begin{matrix} \tau & 1 \\ \eta, L & 1 \end{matrix} \middle| \begin{matrix} \tau' \\ \eta', L' \end{matrix} \right\rangle \delta_{N'\,N+1}\delta_{n_d'\,n_d+1}, \tag{A1}$$

where after the $\sqrt{N+1}$ factor on the right-hand side of Eq. (A1), the first, the second, and the third factors are the elementary Wigner coefficient of U(6) ⊃ U(5), U(5) ⊃ O(5), and O(5) ⊃ SO(3), respectively, which have already been known [30–32]. The same equation applies to reduced matrix elements of the $D^\dagger$ operator in its own basis as well. In the calculation, the relations

$$\langle N'\, n_d'\, \tau'\, \eta'\, L' \| \tilde{d} \| N\, n_d\, \tau\, \eta\, L\rangle = (-1)^{L-L'}\sqrt{\tfrac{2L+1}{2L'+1}}\langle N\, n_d\, \tau\, \eta\, L \| d^\dagger \| N'\, n_d'\, \tau'\, \eta'\, L'\rangle \tag{A2}$$

and

$$\left\langle \begin{matrix} \tau' & 1 \\ \eta', L' & 2 \end{matrix} \middle| \begin{matrix} \tau \\ \eta, L \end{matrix} \right\rangle = (-1)^{L-L'}\sqrt{\frac{\dim(\tau)(2L'+1)}{\dim(\tau')(2L+1)}}\left\langle \begin{matrix} \tau & 1 \\ \eta, L & 2 \end{matrix} \middle| \begin{matrix} \tau' \\ \eta', L' \end{matrix} \right\rangle \tag{A3}$$

may be used, in which

$$\dim(\tau) = (\tau+1)(\tau+2)(2\tau+3)/6 \tag{A4}$$

is the dimension of the O(5) irrep $(\tau, 0)$.

Accordingly, the reduced matrix elements of $\hat{Q}^{(0)}(k)$ in its own basis are given by

$$\begin{aligned}
&\langle N+2k\, n_d'\, \tau'\, \eta'\, L' \| \hat{Q}^{(0)}(k) \| N+2k\, n_d\, \tau\, \eta\, L\rangle \\
&= \left\langle \begin{matrix} \tau & 1 \\ \eta, L & 1 \end{matrix} \middle| \begin{matrix} \tau' \\ \eta', L' \end{matrix} \right\rangle \Bigg(\sqrt{(N+2k-n_d)(n_d+1)} \left\langle \begin{matrix} n_d, & 1 \\ \tau & 1 \end{matrix} \middle| \begin{matrix} n_d+1 \\ \tau' \end{matrix} \right\rangle \delta_{n_d',\, n_d+1} \\
&\quad + \sqrt{(N+2k-n_d+1)\, n_d}\sqrt{\frac{\dim(\tau)}{\dim(\tau')}} \left\langle \begin{matrix} n_d-1 & 1 \\ \tau' & 1 \end{matrix} \middle| \begin{matrix} n_d \\ \tau \end{matrix} \right\rangle \delta_{n_d',\, n_d-1} \Bigg) \\
&\quad + \chi_k\, n_d \delta_{n_d',\, n_d} \sum_{\tau''\eta''L''} (-1)^{L'+L''}\sqrt{5(2L+1)} \left\{ \begin{matrix} L' & 2 & L'' \\ 2 & L & 2 \end{matrix} \right\} \left\langle \begin{matrix} n_d-1 & 1 \\ \tau'' & 1 \end{matrix} \middle| \begin{matrix} n_d \\ \tau' \end{matrix} \right\rangle \left\langle \begin{matrix} n_d-1 & 1 \\ \tau'' & 1 \end{matrix} \middle| \begin{matrix} n_d \\ \tau \end{matrix} \right\rangle \left\langle \begin{matrix} \tau'' & 1 \\ \eta'', L'' & 2 \end{matrix} \middle| \begin{matrix} \tau \\ \eta, L \end{matrix} \right\rangle \left\langle \begin{matrix} \tau'' & 1 \\ \eta'', L'' & 2 \end{matrix} \middle| \begin{matrix} \tau' \\ \eta', L' \end{matrix} \right\rangle
\end{aligned} \tag{A5}$$

for $k = 0$ or 1, which applies to evaluate reduced matrix elements of the $\hat{Q}^{(1)}(k)$ operator in its own basis as well. Using the Wigner-Racah calculus, we have that

$$\begin{aligned}&\langle N + 2k\, n'_d\, \tau'\, \eta'\, L \| \hat{Q}^{(0)}(k) \cdot \hat{Q}^{(0)}(k) \| N + 2k\, n_d\, \tau\, \eta\, L \rangle \\ &= \sum_{n''_d, \tau'', \eta'', L''} (-1)^{L''-L} \sqrt{\frac{2L''+1}{2L+1}} \langle N + 2k\, n'_d\, \tau'\, \eta'\, L \| \hat{Q}^{(0)}(k) \| N + 2k\, n''_d\, \tau''\, \eta'', L'' \rangle \\ &\quad \times \langle N + 2k\, n''_d\, \tau''\, \eta'', L'' \| \hat{Q}^{(0)}(k) \| N + 2k\, n_d\, \tau\, \eta\, L \rangle, \end{aligned} \tag{A6}$$

which also applies to evaluate reduced matrix elements of the $\hat{Q}^{(1)}(k) \cdot \hat{Q}^{(1)}(k)$ operator in its own basis. Similarly, we also have that

$$\begin{aligned}&\langle N + 2k\, n'_d\, \tau'\, \eta'\, L'_0; \mathscr{N}\, n'_{d1}\, \tau'_1\, L'_1; L \| \hat{Q}^{(0)}(k) \cdot \hat{Q}^{(1)}(k) \| N + 2k\, n_d\, \tau\, \eta\, L_0; \mathscr{N}\, n_{d1}\, \tau_1\, L_1; L \rangle \\ &= (-1)^{L'_1+L_0+L} \sqrt{(2L'_0+1)(2L'_1+1)} \begin{Bmatrix} L_0 & L_1 & L \\ L'_1 & L'_0 & 2 \end{Bmatrix} \langle N + 2k\, n'_d\, \tau'\, \eta'\, L'_0 \| \hat{Q}^{(0)}(k) \| N \\ &\quad + 2k\, n_d\, \tau\, \eta\, L_0 \rangle \langle \mathscr{N}\, n'_{d1}\, \tau'_1\, L'_1 \| \hat{Q}^{(1)}(k) \| \mathscr{N}\, n_{d1}\, \tau_1\, L_1 \rangle, \end{aligned} \tag{A7}$$

$$\begin{aligned}&\langle N + 2k\, n'_d\, \tau'\, \eta'\, L \| [\hat{Q}^{(0)}(k) \cdot \tilde{D} + \tilde{D} \cdot \hat{Q}^{(0)}(k)] \| N + 2k\, n_d\, \tau\, \eta\, L_0; 1\,1\,1\,2; L \rangle \\ &= \langle N + 2k\, n_d\, \tau\, \eta\, L_0; 1\,1\,1\,2; L \| [\hat{Q}^{(0)}(k) \cdot D^\dagger + D^\dagger \cdot \hat{Q}^{(0)}(k)] \| N + 2k\, n'_d\, \tau'\, \eta'\, L \rangle \\ &= 2 \langle N + 2k\, n'_d\, \tau'\, \eta'\, L \| \hat{Q}^{(0)}(k) \| N + 2k\, n_d\, \tau\, \eta, L_0 \rangle, \end{aligned} \tag{A8}$$

and

$$\langle N + 2k\, n'_d\, \tau'\, \eta'\, L; 0\,0\,0\,0; L \| [\hat{Q}^{(1)}(k) \cdot \tilde{D} + \tilde{D} \cdot \hat{Q}^{(1)}(k)] \| N + 2k\, n_d\, \tau\, \eta\, L_0; 1\,1\,1\,2; L \rangle = 0. \tag{A9}$$

In calculating reduced matrix elements of the $T(\mathrm{E2})$ operator, we also need

$$\begin{aligned}&\langle N + 2k\, n'_d\, \tau'\, \eta'\, L'_0; \mathscr{N}\, n'_{d1}\, \tau'_1\, L'_1; L' \| \hat{Q}^{(0)}(k) \| N + 2k\, n_d\, \tau\, \eta\, L_0; \mathscr{N}\, n_{d1}\, \tau_1\, L_1; L \rangle \\ &= (-1)^{L'_1+L_1+L} \sqrt{(2L'_0+1)(2L+1)} \begin{Bmatrix} L' & L_1 & L'_0 \\ L_0 & 2 & L \end{Bmatrix} \\ &\quad \times \langle N + 2k\, n'_d\, \tau'\, \eta'\, L'_0 \| \hat{Q}^{(0)}(k) \| N + 2k\, n_d\, \tau\, \eta\, L_0 \rangle \delta_{n'_{d_1} n_{d_1}} \delta_{\tau'_1 \tau_1} \delta_{L'_1 L_1}, \end{aligned} \tag{A10}$$

$$\begin{aligned}&\langle N + 2k\, n'_d\, \tau'\, \eta'\, L'_0; \mathscr{N}\, n'_{d1}\, \tau'_1\, L'_1; L' \| \hat{Q}^{(1)}(k) \| N + 2k\, n_d\, \tau\, \eta\, L_0; \mathscr{N}\, n_{d1}\, \tau_1\, L_1; L \rangle \\ &= (-1)^{L'+L_0+L_1} \sqrt{(2L'_1+1)(2L+1)} \begin{Bmatrix} L' & L_0 & L'_1 \\ L_1 & 2 & L \end{Bmatrix} \langle \mathscr{N}\, n'_{d1}\, \tau'_1\, L'_1 \| \hat{Q}^{(1)}(k) \| \mathscr{N}\, n_{d1}\, \tau_1\, L_1 \rangle \delta_{n'_d n_d} \delta_{\tau' \tau} \delta_{L'_0 L_0}, \end{aligned} \tag{A11}$$

$$\begin{aligned}&\langle N + 2k\, n'_d\, \tau'\, \eta'\, L'_0; \mathscr{N}'\, n'_{d1}\, \tau'_1\, L'_1; L' \| (\hat{D}^\dagger + \tilde{D}) \| N + 2k\, n_d\, \tau\, \eta\, L_0; \mathscr{N}\, n_{d1}\, \tau_1\, L_1; L \rangle \\ &= (-1)^{L'+L_0+L_1} \sqrt{(2L'_1+1)(2L+1)} \begin{Bmatrix} L' & L_0 & L'_1 \\ L_1 & 2 & L \end{Bmatrix} \langle \mathscr{N}'\, n'_{d1}\, \tau'_1\, L'_1 \| (\hat{D}^\dagger + \tilde{D}) \| \mathscr{N}\, n_{d1}\, \tau_1\, L_1 \rangle \delta_{n'_d n_d} \delta_{\tau' \tau} \delta_{L'_0 L_0}. \end{aligned} \tag{A12}$$

$B(E2; L_\xi \to L'_{\xi'})$ and electric quadrupole moment $Q(L_\xi)$ are given by

$$B(E2; L_\xi \to L'_{\xi'}) = (q_2)^2 \frac{2L'+1}{2L+1} |\langle L'_{\xi'} || \hat{Q} || L_\xi \rangle|^2 \tag{A13}$$

and

$$Q(L_\xi) = \sqrt{\tfrac{16\pi}{5}} q_2 \langle LL,\ 20 | LL \rangle \langle L_\xi || \hat{Q} || L_\xi \rangle, \tag{A14}$$

respectively, where the SO(3) reduced matrix element is defined in terms of the SO(3) Clebsch-Gordan coefficient.

[1] A. Bohr and B. R. Mottelson, *Nuclear Structure* (World Scientific, Singapore, 1998), Vols. 1 and 2.

[2] F. Iachello and A. Arima, *The Interacting Boson Model* (Cambridge University, Cambridge, England, 1987).

[3] D. Bonatsos, *Interacting Boson Models of Nuclear Structure* (Clarendon Press, Oxford, 1988).

[4] P. D. Duval and B. R. Barrett, Phys. Lett. B **100**, 223 (1981); Nucl. Phys. A **376**, 213 (1982).

[5] K. Heyde, P. Van Isacker, M. Waroquier, J. L. Wood, and R. A. Meyer, Phys. Rep. **102**, 291 (1983); J. L. Wood, K. Heyde, W. Nazarewicz, M. Huyse, and P. Van Duppen, *ibid.* **215**, 101 (1992).

[6] K. Heyde and J. L. Wood, Rev. Mod. Phys. **83**, 1467 (2011); **83**, 1655(E) (2011).
[7] G. Rosensteel and D. J. Rowe, Phys. Rev. Lett. **38**, 10 (1977).
[8] D. J. Rowe, Prog. Part. Nucl. Phys. **37**, 265 (1996).
[9] K. D. Launey, T. Dytrych, and J. P. Draayer, Prog. Part. Nucl. Phys. **89**, 101 (2016).
[10] T. Dytrych, K. D. Sviratcheva, C. Bahri, J. P. Draayer, and J. P. Vary, Phys. Rev. Lett. **98**, 162503 (2007); T. Dytrych, K. D. Launey, J. P. Draayer, P. Maris, J. P. Vary, E. Saule, U. Catalyurek, M. Sosonkina, D. Langr, and M. A. Caprio, *ibid.* **111**, 252501 (2013); T. Dytrych, K. D. Launey, J. P. Draayer, D. J. Rowe, J. L. Wood, G. Rosensteel, C. Bahri, D. Langr, and R. B. Baker, *ibid.* **124**, 042501 (2020).
[11] A. E. McCoy, M. A. Caprio, T. Dytrych, and P. J. Fasano, Phys. Rev. Lett. **125**, 102505 (2020).
[12] F. Pan, Y. Zhang, L. Dai, J. P. Draayer, and D. Kekejian, Phys. Lett. B **848**, 138340 (2024).
[13] F. Pan, D. Li, G. Cheng, Z. Qiao, J. Bai, and J. P. Draayer, Phys. Rev. C **97**, 034316 (2018); F. Pan, S. Yuan, Z. Qiao, J. Bai, Y. Zhang, and J. P. Draayer, *ibid.* **97**, 034326 (2018).
[14] T. Thomas, V. Werner, J. Jolie, K. Nomura, T. Ahn, N. Cooper, H. Duckwitz, A. Fitzler, C. Fransen, A. Gade, M. Hinton, G. Ilie, K. Jessen, A. Linnemann, P. Petkov, N. Pietralla, and D. Radeck, Nucl. Phys. A **947**, 203 (2016).
[15] E. Maya-Barbecho, S. Baid, J. M. Arias, and J. E. García-Ramos, Phys. Rev. C **108**, 034316 (2023).
[16] G. Rosensteel and D. J. Rowe, Phys. Rev. Lett. **47**, 223 (1981).
[17] D. J. Rowe and G. Rosensteel, Phys. Rev. C **25**, 3236 (1982).
[18] R. Le Blanc, J. Carvalho, and D. J. Rowe, Phys. Lett. B **140**, 155 (1984).
[19] T. Kibédi and R. H. Spear, At. Data Nucl. Data Tables **89**, 77 (2005).
[20] R. F. Casten, M. Wilhelm, E. Radermacher, N. V. Zamfir, and P. von Brentano, Phys. Rev. C **57**, R1553 (1998).
[21] F. Pan, T. Wang, Y.-S. Huo, and J. P. Draayer, J. Phys. G: Nucl. Part. Phys. **35**, 125105 (2008).
[22] K. Yoshida and T. Nakatsukasa, Phys. Rev. C **88**, 034309 (2013).
[23] J. Kvasil, V. O. Nesterenko, A. Repko, W. Kleinig, and P.-G. Reinhard, Phys. Rev. C **94**, 064302 (2016).
[24] G. Colò, D. Gambacurta, W. Kleinig, J. Kvasil, V. O. Nesterenko, and A. Pastore, Phys. Lett. B **811**, 135940 (2020).
[25] NuDat 3.0, National Nuclear Data Center (Brookhaven National Laboratory), http://www.nndc.bnl.gov/nudat3.
[26] M. Zielińska, T. Czosnyka, J. Choiński, J. Iwanicki, P. Napiorkowski, J. Srebrny, Y. Toh, M. Oshima, A. Osa, Y. Utsuno, Y. Hatsukawa, J. Katakura, M. Koizumi, M. Matsuda, T. Shizuma, M. Sugawara, T. Morikawa, H. Kusakari, A. D. Efimov, and V. M. Mikhajlov, Nucl. Phys. A **712**, 3 (2002).
[27] K. B. Howard, arXiv:2004.02362.
[28] K.B. Howard, U. Garg, M. Itoh, H. Akimune, M. Fujiwara, T. Furuno, Y. K. Gupta, M. N. Harakeh, K. Inaba, Y. Ishibashi, K. Karasudani, T. Kawabata, A. Kohda, Y. Matsuda, M. Murata, S. Nakamura, J. Okamoto, S. Ota, J. Piekarewicz, A. Sakaue *et al.*, Phys. Lett. B **807**, 135608 (2020).
[29] B. G. Wybourne, *Classical Groups for Physicists* (Wiley, New York, 1974).
[30] P. Van Isacker, A. Frank, and H.-Z. Sun, Ann. Phys. **157**, 183 (1984).
[31] D. J. Rowe, P. S. Turner, and J. Repka, J. Math. Phys. **45**, 2761 (2004).
[32] F. Pan, L. Bao, Y.-Z. Zhang, and J. P. Draayer, Eur. Phys. J. Plus **129**, 169 (2014).